JACS
JOURNAL OF THE AMERICAN CHEMICAL SOCIETY
Article
pubs.acs.org/JACS

Dinitrosyl Iron Complexes with Cysteine. Kinetics Studies of the Formation and Reactions of DNICs in Aqueous Solution

José Clayston Melo Pereira,[†,‡] Alexei V. Iretskii,[†,§] Rui-Min Han,*[,†,∥] and Peter C. Ford*[,†]

[†]Department of Chemistry and Biochemistry, University of California, Santa Barbara, Santa Barbara, California 93106-9510, United States

[‡]Departamento de Química Geral e Inorgânica, Instituto de Química de Araraquara, UNESP – Universidade Estadual Paulista, Araraquara, São Paulo 14801−970, Brazil

[§]Department of Chemistry and Environmental Sciences, Lake Superior State University, Sault Sainte Marie, Michigan 49783, United States

[∥]Department of Chemistry, Renmin University of China, 59 ZhongGuanCun St., Beijing, 100872, China

Supporting Information

ABSTRACT: Kinetics studies provide mechanistic insight regarding the formation of dinitrosyl iron complexes (DNICs) now viewed as playing important roles in the mammalian chemical biology of the ubiquitous bioregulator nitric oxide (NO). Reactions in deaerated aqueous solutions containing $FeSO_4$, cysteine (CysSH), and NO demonstrate that both the rates and the outcomes are markedly pH dependent. The dinuclear DNIC $Fe_2(\mu\text{-CysS})_2(NO)_4$, a Roussin's red salt ester (**Cys-RSE**), is formed at pH 5.0 as well as at lower concentrations of cysteine in neutral pH solutions. The mononuclear DNIC $Fe(NO)_2(CysS)_2^-$ (**Cys-DNIC**) is produced from the same three components at pH 10.0 and at higher cysteine concentrations at neutral pH. The kinetics studies suggest that both **Cys-RSE** and **Cys-DNIC** are formed via a common intermediate $Fe(NO)(CysS)_2^-$. **Cys-DNIC** and **Cys-RSE** interconvert, and the rates of this process depend on the cysteine concentration and on the pH. Flash photolysis of the **Cys-RSE** formed from Fe(II)/NO/cysteine mixtures in anaerobic pH 5.0 solution led to reversible NO dissociation and a rapid, second-order back reaction with a rate constant $k_{NO} = 6.9 \times 10^7\ M^{-1}\ s^{-1}$. In contrast, photolysis of the mononuclear-DNIC species **Cys-DNIC** formed from Fe(II)/NO/cysteine mixtures in anaerobic pH 10.0 solution did not labilize NO but instead apparently led to release of the $CysS^{\bullet}$ radical. These studies illustrate the complicated reaction dynamics interconnecting the DNIC species and offer a mechanistic model for the key steps leading to these non-heme iron nitrosyl complexes.

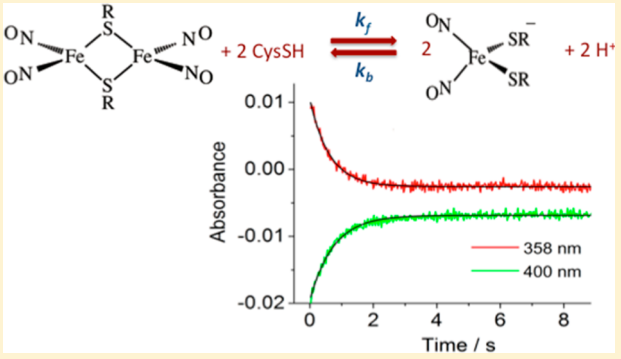

INTRODUCTION

Nitric oxide (nitrogen monoxide, NO) is an bioregulator that has important roles in mammalian physiological functions such as vasodilation, inflammation, neuronal transmission, and immune system response.[1] Other NO derivatives, such as S-nitrosothiols (RSNO) and N-nitrosoamines (R_2NNO), heme and non-heme iron nitrosyl complexes as well as the oxidation products, NO_2^-, $ONOO^-$, and NO_3^- also have physiological presence, and their specific roles remain the subjects of continuing studies. The dinitrosyl iron complexes (DNICs) comprise one class of such species. DNICs are four-coordinate $Fe(NO)_2L_2^{n\pm}$ complexes thought to be formed from the chelatable iron pool, thiol-containing ligands (for example, glutathione, cysteine, or protein thiol), and endogenous or exogenous NO.[2] Although DNICs were first discovered some decades ago,[3−6] there has been a recent upsurge of interest in the biological or pathological pathways to which these species contribute.[2,7−15]

Previous studies have demonstrated reversible transformations between the Roussin's red salt ester analogs $Fe_2(\mu\text{-RS})_2(NO)_4$,[6] which are binuclear DNICs, and mononuclear species $[Fe(NO)_2L_2]^{n\pm}$ (Figure 1). In aqueous media, these

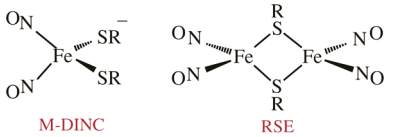

Figure 1. Generic formulas for a mononuclear dinitrosyl iron complex (M-DNIC) (left) and for the binuclear DNIC, a Roussin's red salt ester, (RSE) (right). In the present case, the thiolate RS^- is the cysteinate anion, and the M-DNIC $Fe(NO)_2(CysS)_2^-$ is designated as **Cys-DNIC** and the RSE $Fe_2(\mu\text{-Cys})_2(NO)_4$ is designated as **Cys-RSE**.

Received: October 16, 2014
Published: December 5, 2014

   dx.doi.org/10.1021/ja510393q | J. Am. Chem. Soc. 2015, 137, 328−336

equilibria are dependent on both pH and thiol ligand concentration.[9] The dinuclear species is the dominant form at lower pH, while the mononuclear complex predominates at higher pH. However, there is relatively little quantitative information regarding the dynamics of the formation and interconversion of these DNICs.[14] The present stopped-flow and flash photolysis kinetics study was initiated to address this issue.

RESULTS AND DISCUSSION

The present studies use aqueous ferrous sulfate as the iron source, purified NO gas, and L-cysteine (CysSH) in order to model the formation of biological DNICs. In each case the solutions were deaerated in order to avoid the autoxidation of NO. In discussing the reactions of these species in aqueous solutions, it is important to remember that this system involves a number of dynamic pH-dependent equilibria involving various iron complexes as well as that between CysSH and its conjugate base $CysS^-$. In this context, kinetics experimental conditions are reported in terms of the following variables: $[Fe]_{tot}$ = the total concentration of iron(II) introduced to the system; $[Cys]_{tot}$ = the total concentration of L-cysteine introduced, $\sim([CysSH] + [CysS^-])$ since $[Cys]_{tot}$ is generally $\gg [Fe]_{tot}$; and $[NO]_{tot}$ = the solution nitric oxide concentration, based on the total amount of NO introduced to the system and the partition coefficient between the gas and liquid phases.

Spectra of Fe/NO/CysSH Solutions at Various pH. The earlier study by Vanin and co-workers[9] reported that the binuclear DNIC $Fe_2(\mu\text{-CysS})_2(NO)_4$ (**Cys-RSE**) is the dominant iron-containing species in such solutions at low pH. This was confirmed by recording the optical spectrum of a deaerated solution containing Fe(II) (0.18 mM), NO (0.93 mM), and CysSH (5.4 mM) in pH 5.0 citrate buffer. This spectrum (Figure 2, top) displayed the two absorption bands (312 and 362 nm) with a shoulder (434 nm) reported[9a] for **Cys-RSE** and characteristic of that for other RSEs.[16,17] In contrast, a deaerated pH 10.0 borate buffer solution prepared from Fe(II) (0.18 mM), NO (0.93 mM), and CysSH (1.8 mM) displayed a spectrum (Figure 2, top) with a single band centered at 400 nm as reported[9a] for **Cys-DNIC**. In pH 7.4 HEPES buffer, a spectrum analogous to that of **Cys-RSE** was seen for $[CysSH]_{tot}$ = 1.8 mM, while one close to that of **Cys-DNIC** was seen for $[CysSH]_{tot}$ = 18.0 mM under otherwise analogous conditions (Figure 2, bottom). None of these features are apparent in the spectra of analogous deaerated solutions of Fe^{2+} alone, of cysteine alone, or of Fe^{2+} and CysSH together in pH 5 citrate buffer, in pH 7.4 HEPES buffer or in pH 10 borate buffer (Supporting Information (SI) Figure S-1).

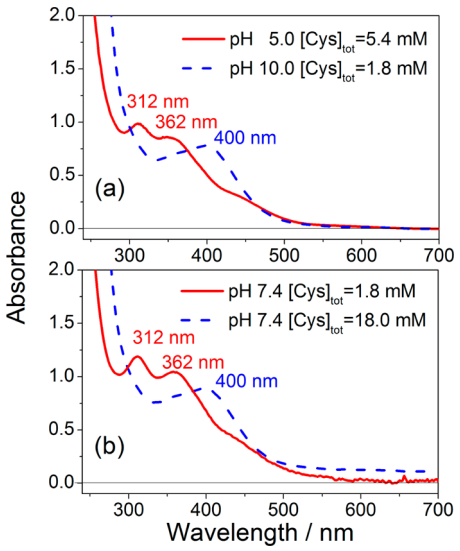

Figure 2. Top: Absorption spectra of **Cys-RSE** (red line) formed from Fe(II) ($[Fe]_{tot}$ = 0.18 mM) and NO ($[NO]_{tot}$ = 0.93 mM) with CysSH ($[Cys]_{tot}$ =5.4 mM) at pH 5.0 citrate buffer and **Cys-DNIC** (dashed blue) formed from the mixture of Fe(II) (0.18 mM) and NO (0.93 mM) with CysSH (1.8 mM) at pH 10.0 borate buffer. Bottom: Spectra at pH 7.4 (HEPES buffer) with CysSH at 1.8 mM (red) and at 18.0 mM (dashed blue). In all cases the solutions were deaerated.

The EPR spectrum recorded for a solution prepared from ferrous sulfate ($[Fe]_{tot}$ = 0.18 mM), CysSH ($[Cys]_{tot}$ = 20 mM), and NO ($[NO]_{tot}$ = 1.86 mM) in deaerated pH 7.4 HEPES buffer (100 mM) indicated the presence of a paramagnetic species with g_{ave} = 2.03 (SI Figure S-2). This was essentially identical to the EPR spectrum reported by Vanin et al.[9c] for an analogous solution and attributed by these workers to the mononuclear DNIC formed from cysteinate, that is, **Cys-DNIC**. Similar EPR spectral signatures have been noted by others[17,18] and are considered to be diagnostic of thiolate coordinated DNIC anions of the type $Fe^{I}(NO)_2(RS)_2^-$. When a less than stoichiometric NO concentration was used ($[NO]_{tot}$ = 0.093 mM), the EPR spectrum was still dominated by the signal for Cys-DNIC with g = 2.03. However, a weaker signal with g = 2.04 was also evident (SI Figure S-3) similar to one that Vanin et al.[9c] have attributed to a triplet mononitrosyl iron complex, presumably $Fe(NO)(CysS)_2^-$ in the present case.[18,19] Notably, DFT computations suggest that the mononitrosyl iron intermediate $Fe^{I}(NO)(CysS)(H_2O)_2$ intermediate also has an S = 1 electronic configuration (see below).

Kinetics Studies at pH 5.0: Formation of Cys-RSE. At this pH, the overall reaction to form **Cys-RSE** from a solution containing Fe(II), NO, and CysSH was quite slow, so optical spectral changes were monitored using a conventional UV−vis spectrophotometer (Figure 3). A solution of Fe(II) (0.18 mM) and CysSH (5.4 mM) was prepared in a deaerated Schlenk cuvette,[20] and it is notable that the resulting spectrum did not display obvious differences from the spectra of solutions of Fe(II) and of CysSH alone, suggesting that there was little

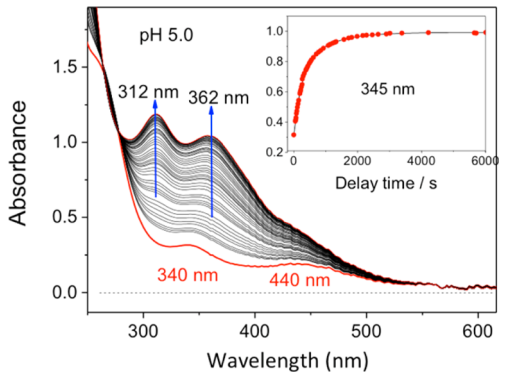

Figure 3. Spectral changes seen in pH 5.0 (100 mM citrate buffer) upon adding NO to a deaerated solution of Fe(II) and CysSH to give the final concentrations $[Fe]_{tot}$ = 0.18 mM, $[CysSH]_{tot}$ = 5.4 mM, and $[NO]_{tot}$ = 1.86 mM. The inset shows the temporal absorbance at λ_{mon} = 345 nm.

dx.doi.org/10.1021/ja510393q | J. Am. Chem. Soc. 2015, 137, 328−336

complex formation between Fe^{2+} and CysSH under these conditions. However, immediately upon adding NO (P_{NO} = 1 atm) and shaking the solution to give a NO concentration of 1.86 mM (based upon the solubility of NO in water),[21] the spectrum displayed two bands with maxima at 340 and 440 nm (Figure 3). These bands are ascribed to rapid formation of $Fe(H_2O)_5(NO)^{2+}$ ($FeNO^{2+}$, eq 1), which was shown by Wannet et al. to be formed from aqueous Fe(II) and NO with a relatively small equilibrium constant K_{NO} (1.15×10^3 M^{-1} in pH 5.0, acetate buffer, 23 °C)[22] but with a large second-order rate constant $k_{NO} = 1.4 \times 10^6$ M^{-1} s^{-1}. The solution spectrum then continued to evolve over a period of minutes to give a final, stable spectrum that can be ascribed to that of **Cys-RSE** (Figures 2 and 3).

$$Fe(H_2O)_6^{2+} + NO \overset{K_{NO}}{\rightleftharpoons} Fe(H_2O)_5(NO)^{2+} + H_2O \qquad (1)$$

The absorbance changes of the type shown in Figure 3 can be fit to an exponential function to obtain k_{obs} values indicating the reaction to be first order in the iron substrate. However, at lower values of P_{NO} in the cuvette, a feature characteristic of systems depending on gas/liquid transport was apparent. The gas phase volume in the cuvette was about 8 times that of the liquid phase, and therefore, given NO's low aqueous solubility (1.86 mM atm^{-1} at 298 K),[21] the vast majority of the nitric oxide present in the system for any experiment is in the gas phase. Thus, at lower P_{NO}, the solution phase NO concentration is no longer in such excess over $[Fe]_{tot}$ that the [NO] remains effectively constant throughout the experiment, unless adequate provision is made to ensure that the gas and liquid phases remain in equilibrium. For a slow reaction, this can be done by periodically shaking the cell, under such conditions, the temporal absorbance changes are exponential (see SI Figure S-4), and this leads to the conclusion that the reaction being observed is first order in [Fe(II)]. However, for the faster reactions, an alternative approach is to measure the initial rates, since these are established for the initial reaction conditions. The latter approach was taken for most of the experiments described in this section.

Figure 4 illustrates the results of kinetics experiments in pH 5.0 solution systematically studied as functions of the cysteine and NO concentrations. When $[Cys]_{tot}$ was varied over the range 0–27.0 mM with $[NO]_{tot}$ (0.93 mM) and $[Fe]_{tot}$ (0.18 mM) held constant, the initial rates proved to be a linear function of $[Cys]_{tot}$ squared. Notably, the kinetics behaviors of these relatively slow reactions were essentially indistinguishable whether the Fe(II) and the NO were premixed and the CysSH was then added or the Fe(II) and the CysSH were premixed and the NO was then introduced. This behavior is consistent with the view that, under these conditions, the reactions before the rate-limiting step are rapidly established pre-equilibria. Figure 4 (bottom) illustrates the effect of $[NO]_{tot}$ on the initial rates over the range 0–1.5 mM with $[Cys]_{tot}$ (5.4 mM) and $[Fe]_{tot}$ (0.18 mM) held constant. Notably the latter plot is nonlinear, leveling off at higher values of [NO], an observation consistent with an equilibrium such as that described by eq 1. The curve fit shown in Figure 4 (bottom) is according to eq 2, with the values $C_1 = (1.19 \pm 0.24) \times 10^2$ M^{-3} L^{-1} s^{-1} and $C_2 = (6.2 \pm 2.0) \times 10^2$ M^{-1}. Notably, the value for C_2 falls within the range of values (440–1150 M^{-1}) reported for the equilibrium constant (K_{NO}) for eq 1 under similar conditions.[22b]

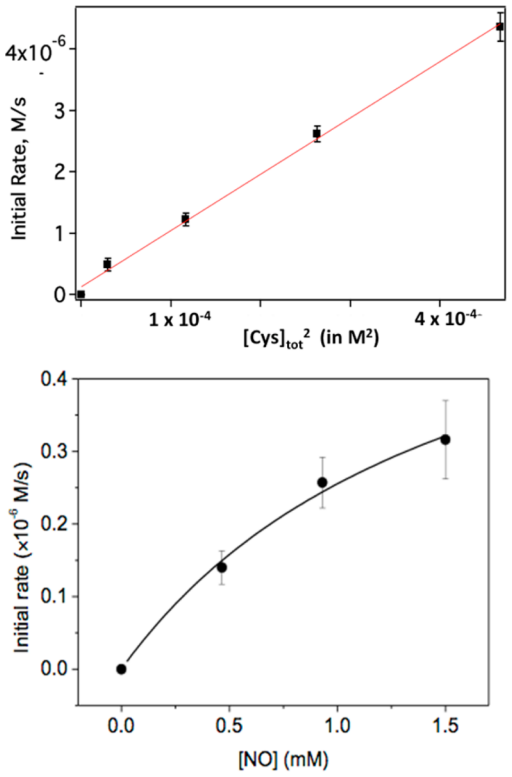

Figure 4. Initial rates as functions of $[Cys]_{tot}$ and of $[NO]_{tot}$ from mixing Fe(II), CysSH, and NO in pH 5.0 (100 mM citrate buffer), T = 298 K. Top: Initial rates vs $[Cys]_{tot}^2$ ($[Fe]_{tot}$ = 0.18 mM; [NO] = 0.93 mM. Bottom: Initial rates vs [NO] ($[Fe]_{tot}$ = 0.18 mM; $[NO]_{tot}$ = 0, 0.5, 1.0, and 1.5 mM; $[Cys]_{tot}$ = 5.4 mM). The curve is a fit of the data according to form of eq 2, see text.

$$\text{rate} = C_1C_2[Cys]_{tot}^2[Fe]_{tot}[NO]/(1 + C_2[NO]) \qquad (2)$$

The sequence of processes represented by **Cys-RSE** formation from a solution mixture of Fe(II), CysSH and NO must be very intricate, requiring the substitution of several components into the coordination sphere of the iron, the reduction of Fe(II) to Fe(I), and the assembly of two iron/cysteinate/nitrosyl units into the dimeric structure. In this context, the first point to take into consideration is that, given the relative lability of iron(II) complexes,[22,23] it is very unlikely that the slow formation of **Cys-RSE** at pH 5.0 seen in Figure 3 is rate limited by simple substitution into the coordination sphere of the Fe^{2+} ion. This leads us to propose that reduction of Fe(II) is the rate-limiting process. A scenario consistent with the rate law described by eq 2 is outlined in Scheme 1.

In Scheme 1, the rate-limiting step (eq 5) is proposed to be a spontaneous reduction of the Fe(II) center of $Fe(NO)(CysS)_2$ (**C**, the remaining coordination sites being occupied by waters) to give the Fe(I) intermediate **D** plus a cysteinyl radical $CysS^{\bullet}$. **C** would be formed reversibly by reaction of the ferrous center with NO and two cysteines (eq 1 and eqs 3 and 4 in Scheme 1) by relatively fast substitutions for the coordinated waters of the Fe(II) center. The equilibria represented by eqs 3 and 4 are certainly very pH dependent, but the data under consideration here were recorded at a single pH (5.0). Thus, at this relatively low pH, the overall concentration of **C** would be small, and the overall rate (k_r[C]) would be relatively slow. As seen below, the reactions are much faster at higher pH. Once **D** is formed, it is likely that it would rapidly capture another NO from the

dx.doi.org/10.1021/ja510393q | J. Am. Chem. Soc. 2015, 137, 328–336

Scheme 1. Proposed Sequence of Reactions Leading to DNIC Products

$$Fe^{2+} + NO \overset{K_{NO}}{\rightleftharpoons} Fe^{II}(NO)^{2+} \quad (A)$$

$$A + CysSH \overset{K_1}{\rightleftharpoons} Fe^{II}(NO)(CysS)^{+} + H^{+} \quad (3)$$
(B)

$$B + CysSH \overset{K_2}{\rightleftharpoons} Fe^{II}(NO)(CysS)_2 + H^{+} \quad (4)$$
(C)

$$C \overset{k_r}{\longrightarrow} Fe^{I}(NO)(CysS) + CysS\bullet \quad (5)$$
(D)

$$D + NO \overset{fast}{\longrightarrow} Fe^{I}(NO)_2(CysS) \quad (6)$$
(E)

$$2\,E \overset{fast}{\longrightarrow} Fe_2(\mu\text{-}CysS)_2(NO)_4 \quad (7)$$
(Cys-RSE)

solution to give a dinitrosyl species **E**, which is a likely precursor to either **Cys-RSE** or **Cys-DNIC**.

An alternative, essentially kinetically equivalent, rate-limiting step at pH 5.0 would be for **B** to undergo outer-sphere reduction by a $CysS^-$ anion to give the same products. However, the stopped flow experiments at higher pH showing a two-stage process, one fast and dependent on $[Cys]_{tot}^2$ and pH and the second being much slower and pH independent (see below), would appear to argue against that alternative. In the presence of excess NO, either reduction pathway should lead to formation of the S-nitroso adduct CysSNO, since $CysS^\bullet$ radical would be trapped by the excess NO. Another essentially kinetically equivalent mechanism at pH 5.0 would be for $CysS^-$ to undergo nucleophilic attack on the coordinated NO of **B** to give a $Fe^I(CysS^-)$ complex plus CysS-NO. Similar reductive reactions have been noted for Fe(III) and Cu(II) complexes.[24] However, this pathway to Fe(I) intermediates would not be consistent with the kinetics data acquired at higher pH (see below).

The reactions outlined by Scheme 1 would give the rate law:

$$\text{rate} = k_r K_1 K_2 [H^+]^{-2} K_{NO} [Cys]_{tot}^2 [NO][Fe]_{tot} / (1 + K_{NO}[NO]) \quad (8)$$

This has the same form as eq 2, if $C_1 = k_r K_1 K_2 [H^+]^{-2}$ and $C_2 = K_{NO}$ and predicts that the overall transformation will be markedly accelerated at higher pH, consistent with the results of the experiments described below. However, it should be noted that this relatively "simple" form of the rate law would be applicable only under the mildly acidic conditions used in the above experiments where pH ≪ pK_a(CysSH) (see SI Scheme S-1)

DFT Studies of eq 5. Figure 5 illustrates the result of DFT computations of the optimized structures of the proposed species **C** and **D** in a dielectric continuum (Scheme 1). All optimizations were performed at unrestricted B3PLYP/DGDZVP level without symmetry constraints using polarizable continuum model (Gaussian 2009) and were starting from "octahedral" geometry with water molecules occupying any coordination sites not taken by NO or the cysteine thiolate anion. (Coordinates for DFT calculated structures of intermediates **C** and **D** are listed in SI Table S-1.) Notably, the optimized structure of species **C** is pentacoordinate

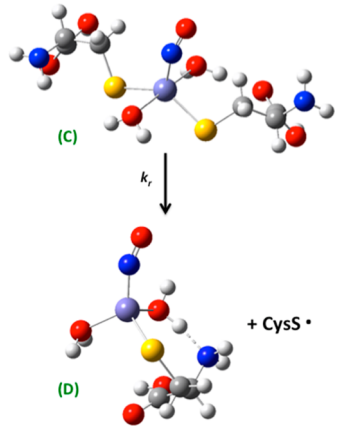

Figure 5. DFT computed structures for the rate-limiting step proposed in Scheme 1.

(pseudo square pyramidal) with a quartet ground state, while the optimized structure of **D** is tetracoordinate (pseudo tetrahedral) with a triplet ground state. A number of other configurations (including structures with S,O bidentate cysteinate ligands) were also investigated, but those shown in Figure 5 proved to be the most energetically likely. The calculated energy difference between the reactants and products of eq 5 (Scheme 1) in a dielectric continuum was +14 kcal mol^{-1}, indicating that this reaction is a thermodynamically reasonable explanation of the kinetics described. Notably, trapping of the $CysS^\bullet$ by NO is calculated to be exothermic by 37 kcal mol^{-1}, thus making the overall process quite favorable.

Kinetics Studies at pH 10.0: Formation of Cys-DNIC, $Fe(NO)_2(CysS)_2^-$. When the analogous experiment was performed in pH 10.0 borate buffer (100 mM), the product spectrum displayed a band centered at ~395 nm indicating the formation of **Cys-DNIC** (Figure 2). The product formation was too fast to monitor by conventional spectroscopy, so the stopped-flow spectroscopic technique was used to follow the temporal absorbance changes at 300−500 nm. When a solution containing $FeSO_4$ (0.36 mM) and excess CysSH (3.6 mM) in nanopure water was rapidly mixed with an equal volume of a solution containing NO (1.86 mM) in pH 10.0 borate buffer (200 mM), two steps were observed. First, there was a rapid increase of absorption at 360 nm over the course of a few milliseconds indicating the formation of a transient intermediate we designate as "**X**", and this was followed by a much slower decrease over a period of a few seconds (Figure 6 inset). The absorbance changes at 360 nm could be fit to a two-stage kinetics model for sequential reactions with exponential functions giving rate constants $k_{obs}(a) = 105 \pm 2\ s^{-1}$ for generation of the first observable intermediate and $k_{obs}(b) = 4.7 \pm 0.1\ s^{-1}$ for formation of **Cys-DNIC** in subsequent steps. These results are summarized in SI Table S-2.

The kinetics data obtained at different observation wavelengths allow one to construct the spectrum of the intermediate(s) formed after the initial reaction. Figure 6 displays the result of using this point-by-point method to obtain the transient spectra at 20 ms and at 2 s from kinetic curves obtained at different wavelengths. The spectrum recorded at 20 ms displays a band centered at 360 nm ascribed to the intermediate "**X**". The spectrum recorded at 2 s displays a band centered at 395 nm, which is consistent with the final spectrum (Figure 2), indicating the rapid formation of **Cys-DNIC** under these conditions. If the initial steps in the reactions of Fe(II),

dx.doi.org/10.1021/ja510393q | J. Am. Chem. Soc. 2015, 137, 328−336

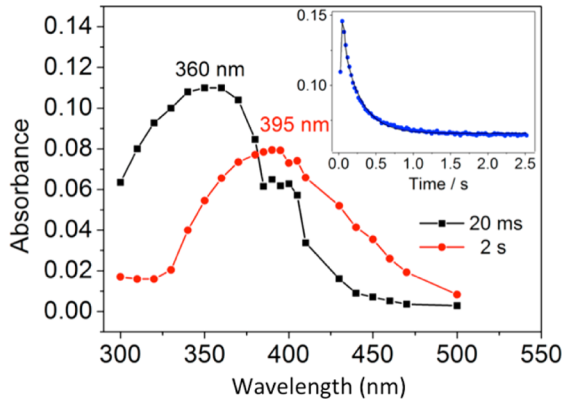

Figure 6. Transient difference spectra recorded at 20 ms (black squares) and at 2 s (red circles) using the point-by-point method with the stopped-flow spectrophotometer when a solution of Fe(II) nanopure water was mixed with a solution of CysSH and NO in pH 10.0 borate buffer, T = 298 K (concentrations after mixing are $[Fe]_{tot}$ = 0.18 mM, $[CysSH]_{tot}$ = 1.8 mM, and $[NO]_{tot}$ = 0.93 mM, 100 mM buffer). Before mixing the solution in the stopped-flow optical path was the solution of Fe(II) in nanopure water. Inset: Typical absorbance changes at 360 nm showing a fast absorbance increase to give an intermediate **X**, followed by slower reaction to form **Cys-DNIC**.

CysSH, and NO at both pH 5 and 10 are described by Scheme 1, then a logical identity of **X** would be as $Fe^{II}(NO)(CysS)_2$, that is, **C**.

Kinetics Studies at pH 7.4. Similar temporal absorbance changes at 360 nm were also observed at pH 7.4 when an analogous solution of Fe(II) and CysSH was mixed in the stopped flow spectrophotometer with a NO/HEPES buffer solution (Figure 7). Again sequential changes were observed

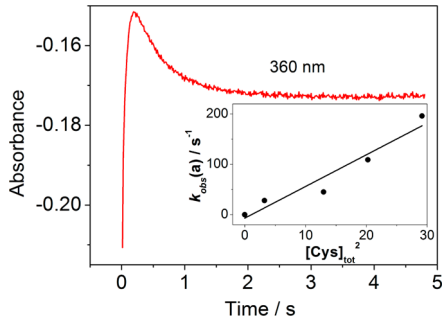

Figure 7. Temporal absorbance changes at 360 nm for the reaction of Fe(II) (0.18 mM), CysSH (1.8 mM), and NO (0.93 mM) in pH 7.4 HEPES buffer (100 mM), T = 298 K. Inset: Plot of rate constants k_{obs}(a) vs $[Cys]_{tot}^2$ for the reaction of Fe(II) (0.18 mM), CysSH (1.8, 3.6, 4.5, and 5.4 mM), and NO (0.93 mM); slope = 6.3 (±0.9) × 10^6 M^{-2} s^{-1}.

with the final spectrum being consistent with the formation of **Cys-DNIC**. For the same initial concentrations of Fe(II), CysSH, and NO, the first step leading to an intermediate proved to be considerably slower (k_{obs}(a) = 28 (±1) s^{-1}) than at pH 10, while the second step displayed a comparable rate constant (k_{obs}(b) = 4.8 (±1.5) s^{-1}). Plots of k_{obs}(a) vs $[Cys]_{tot}^2$ proved to be linear with a slope of 6.3 (±0.9) × 10^6 M^{-2} s^{-1} (Figure 7). In contrast, k_{obs}(b) appears to be independent of the cysteine concentration. This behavior is consistent with the k_{obs}(a) step reflecting formation of the intermediate **C**, as illustrated in Scheme 1.

pH Dependence. As noted above, whether **Cys-DNIC** or **Cys-RSE** is the predominant DNIC formed in Fe/NO/CysSH solutions is dependent both on the solution pH and on $[Cys]_{tot}$. In order to elucidate the pH effect on the reaction dynamics, we probed the temporal absorbance changes at 360 nm as a function of pH. This experiment was carried out by stopped-flow mixing of a solution of Fe(II) and CysSH in nanopure water with an equal volume of a NO solution in various buffers at pH 5.0, 5.6, 6.1, 6.8, 7.4, and 10.0 under anaerobic conditions at 298 K. After mixing, the initial concentrations were $[Fe(II)]_{tot}$ = 0.18 mM, $[CysSH]_{tot}$ = 5.4 mM, $[NO]_{tot}$ = 0.93 mM, and [buffer] = 100 mM. Temporal spectral changes similar to those seen in Figure 7 were observed, but as noted above, the rates of the first step proved to be markedly pH dependent. A plot of the k_{obs}(a) values against pH for the first spectral change (that we have attributed to formation of **C** is shown in Figure 8 (SI Table S-3), although

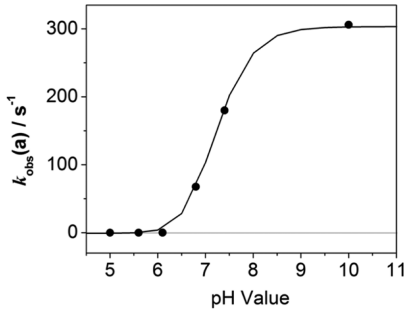

Figure 8. Plot of the rate constants k_{obs}(a) (●) in s^{-1} vs pH values for the reaction of Fe(II) (0.36 mM) and CysSH (10.8 mM) in nanopure water with equal volume of NO solution (1.86 mM) at pH 5.0, 5.6, 6.8, 7.4, and 10.0 buffer (200 mM) at 298 K. Reactant concentrations after mixing were 0.18 mM (Fe(II)), 5.4 mM (CysSH), and 0.93 mM (NO). The line is drawn for illustrative purposes only.

it should be noted that the rate constants given for the lower two pH values are for the overall reaction, since the two stages could not be independently observed. The rates increase markedly as the pH increases, suggesting that the cysteinate anion is the much more reactive form, although the curve drawn through this data suggests a pK_a of ~7.2, perhaps indicating enhanced acidity of coordinated CysSH, given that the pK_a of CysSH is reported as 8.3.[25]

In contrast, the rate constant k_{obs}(b) for the second decay stage, proved to be pH independent (Table S-2). These results are consistent with the first stage of the reaction being the formation of $Fe^{II}(NO)(CysS)_2$ (**C**), The second-order dependence of k_{obs}(a) on $[CysSH]_{tot}$ would imply that eq 4 is rate-limiting in the sequence of steps leading to the intermediate **C** (Scheme 1). Accordingly, the second stage seen in the stopped-flow experiments would be the spontaneous reduction of **C** to **D** followed by rapid reaction of **D** with CysSH and NO to give **Cys-DNIC** at higher pH (eq 9).

$$Fe^{I}(NO)(CysS)(\mathbf{D}) + NO + CysSH \rightarrow Fe(NO)_2(CysS)_2^- + H^+ \quad (9)$$

Interconversion between Cys-RSE and Cys-DNIC at pH 7.4. Cysteine Concentration Dependence. The above data showed that **Cys-RSE** is formed in a pH 7.4 HEPES buffer

dx.doi.org/10.1021/ja510393q | J. Am. Chem. Soc. 2015, 137, 328−336

solution containing Fe(II) (0.18 mM), NO (0.93 mM), and CysSH (1.8 mM). However, at higher [CysSH] (18.0 mM) **Cys-DNIC** is formed (Figure 2) implying that the two species are readily interconverted (eq 10). Similar interconversions have been reported by Tinberg et al.[26] and by Lu et al.[11a] for the addition of excessive thiolates to RSEs.

$$Fe_2(\mu\text{-CysS})_2(NO)_4 + 2CysSH \rightleftharpoons 2Fe(NO)_2(CysS)_2^- + 2H^+ \quad (10)$$

The rates of this interconversion were probed by the stopped-flow mixing of a solution containing mostly **Cys-RSE** in pH 7.4 HEPES buffer ([Cys] = 0.36 mM, [NO] = 1.86 mM) with an equal volume of a pH 7.4 solution containing a large excess of cysteine (36 mM) (final concentrations: $[Fe]_{tot}$ = 0.18 mM; $[Cys]_{tot}$ = 18.2 mM; $[NO]_{tot}$ = 0.93 mM; [buffer] = 100 mM). Under these conditions, the form of the iron complexes shifts almost entirely to **Cys-DNIC**. The exponential absorbance decrease at 358 and the corresponding increase at 400 nm are shown in Figure 9. Plotting the k_{obs}(f) values

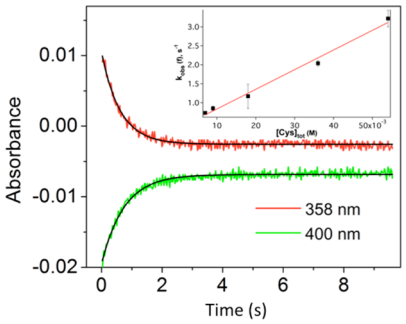

Figure 9. Temporal absorbance changes at 358 nm (red) and 400 nm (green) for the reaction resulting from the stopped-flow mixing of equal volumes of one solution predominately **Cys-RSE** in pH 7.4 HEPES buffer solution (100 mM) containing Fe (0.36 mM), CysSH (0.36 mM) and NO (1.86 mM) and a pH 7.4 of CysSH (36.0 mM) at T = 298 K. The solid lines display the fits of these data to single exponential functions to give the k_{obs}(f) values 1.34 ± 0.03 and 1.62 ± 0.03 s^{-1}, respectively. Insert: Plot of rate constants k_{obs} (s^{-1}) monitored at 400 nm vs $[Cys]_{tot}$ giving the slope k_2 = 52 ± 3.0 M^{-1} s^{-1}.

determined in this manner vs $[Cys]_{tot}$ for different cysteine concentrations proved to be linear with a slope of 52 (±3) M^{-1} s^{-1} and an intercept of 0.03 (±0.01) s^{-1} (see inset of Figure 9). Thus, the rate-limiting step in the conversion of the dinuclear complex **Cys-RSE** to the mononuclear **Cys-DNIC** appears to involve the attack of CysSH (or more likely $CysS^-$) on one of the two iron centers in a step leading to one equivalent of **Cys-DNIC** plus the transient species $Fe^I(CysS)(NO)_2$ (**E**). Rapid reaction of the latter with another CysSH or $CysS^-$ should give a second **Cys-DNIC**.

Based on the above kinetics data, we propose the molecular pathways for the formation of **Cys-RSE** and **Cys-DNIC** and their interconversion as summarized in Scheme 2.

Flash Photolysis Kinetics of Cys-RSE at pH 5.0. Nanosecond kinetic flash photolysis (λ_{ex} 355 nm) was used to investigate the dynamics of the processes resulting from irradiating solutions of **Cys-RSE** formed in pH 5.0 citrate buffer by mixing $FeSO_4$ (0.05 mM), cysteine (2.0 mM), and NO (various concentrations: 0.25, 0.50, 1.00, or 1.50 mM). Figure 10 illustrates one such experiment. At the 400 nm monitoring

Scheme 2. Proposed Scheme for the Formation of $Fe(NO)_2(CysS)_2^-$ (Cys-DNIC) and $Fe_2(\mu\text{-CysS})_2(NO)_4$ (Cys-RSE) and Their Interconversion

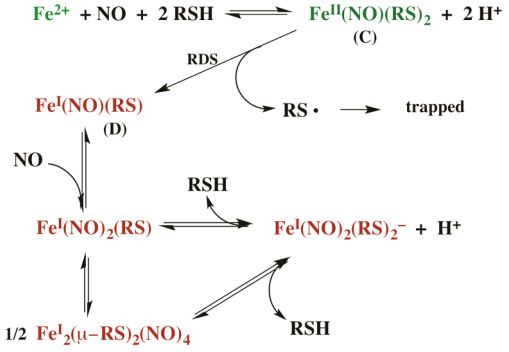

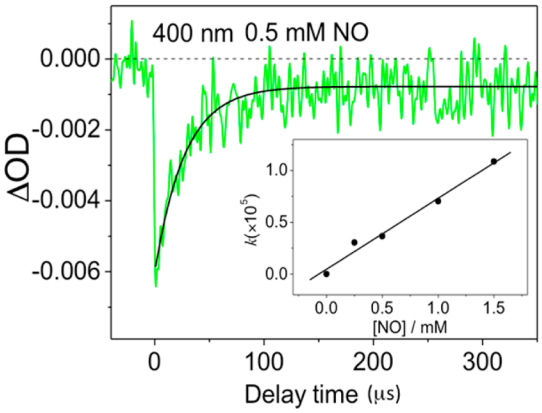

Figure 10. Temporal absorbance changes at 400 nm following 355 nm laser photolysis of the Fe/CysSH/NO species (**Cys-RSE**) formed from a mixture of $FeSO_4$ (0.05 mM), cysteine (2.0 mM), NO (0.50 mM) in pH 5.0 citrate buffer at 298 K. Inset: Plot of k_{obs} vs [NO] for the relaxation of transients formed from the flash photolysis. The slope k_{NO} is 6.9 × 10^7 M^{-1} s^{-1}.

wavelength, flash-induced transient bleaching was immediately apparent, and this was followed by relaxation over several hundred μs back to an absorbance close to that of the original solution. However, the relaxation was only ~91%, complete, and a small fraction of this bleaching does not relax within 1 ms. Absorption spectra recorded before and after the flash experiment (SI Figure S-5) indicated the formation of some long-lived species. Notably control flash photolysis reactions indicated that cysteine itself shows no photochemistry under these conditions or at pH 10.0 (Figure S-6).

The temporal decay of the transient bleaching upon flash photolysis of **Cys-RSE** at pH 5.0 could be fit to single exponential functions (Figure 10), to give the calculated k_{obs} values for different NO concentrations (Table S-4). A plot of these k_{obs} values vs [NO] is linear with an approximately zero intercept (Figure 10 inset). These observations are consistent with photoinduced NO dissociation from **Cys-RSE**, followed by a back reaction of the resulting intermediate with NO (eq 11). Similar reactions have been observed previously for other

$$Fe_2(\mu\text{-CysS})_2(NO)_4 \xrightleftharpoons[k_{NO}]{h\nu} Fe_2(CysS)_2(NO)_3 + NO \quad (11)$$

dx.doi.org/10.1021/ja510393q | J. Am. Chem. Soc. 2015, 137, 328−336

RSEs $Fe_2(\mu\text{-}RS)_2(NO)_4$ (R = $-CH_2CH_2OH$ and $-CH_2CH_2SO_3^-$)[16] as well as for Roussin's red salt anion $Fe_2(\mu\text{-}S)_2(NO)_4^{2-}$.[27] The slope of this line (6.9×10^7 s^{-1} M^{-1}) would be the second-order rate constant k_{NO} value for this relaxation process. Changing $[Cys]_{tot}$ had little effect on k_{obs}, and this observation argues against the possibility that the transient bleaching results from dissociation of a cysteinate moiety.

Flash Photolysis of Cys-DNIC at pH 10.0. Similar nanosecond flash photolysis (λ_{ex} 355 nm) was used to investigate the photochemistry of **Cys-DNIC** formed from mixing $FeSO_4$ (0.05 mM) with cysteine (2.0 mM) and NO (0.05, 0.10, 0.25, 0.50, 0.75, 1.00, or 1.25 mM) in pH 10.0 borate buffer. Again flash photolysis leads to an initial bleach followed by the partial relaxation back to the original absorbance (for example, Figure 11). However, the latter

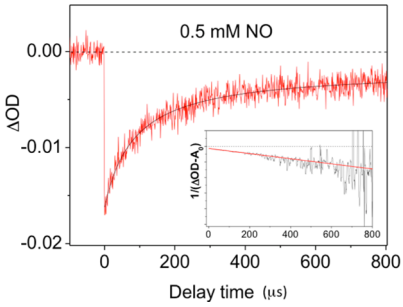

Figure 11. Temporal absorbance changes at 400 nm following 355 nm laser photolysis of the DNIC species formed from a mixture of $FeSO_4$ (0.05 mM), cysteine (20.0 mM), NO (0.50 mM) in pH 10.0 borate buffer at 298 K. Inset: the linear plot of the $1/(\Delta OD - A_0)$ vs time in μs.

process is slower than that seen at the lower pH under otherwise analogous conditions. Furthermore, the temporal absorbance decay curves could not be fit by a simple exponential, but instead fit well with a second-order reaction function giving rate constant k_2 ~10^9 M^{-1} s^{-1} ($\varepsilon_{400\ nm}$(**Cys-DNIC**) = 6.0×10^3 L mol^{-1} cm^{-1}, Table S-5). Although there was some scatter (±20%) in the k_2 values so determined, a 25-fold increase in [NO] from 0.05 mM to 1.25 mM had no effect (SI Figure S-7). Thus, unlike the transient spectral changes at pH 5 attributed to NO dissociation and recombination to regenerate **Cys-RSE** (eq 10), the transient bleaching seen at pH 10 is not due to NO dissociation. Furthermore, varying $[Cys]_{tot}$ from 2.0 to 20 mM led, not to a linear increase in k_2, but instead to a modest, systematic decrease in the relaxation rate constant from 6.6×10^9 to 4.4×10^9 M^{-1} s^{-1} (SI Table S-6, Figure S-8). Thus, $CysS^-$ photodissociation and recombination can also be excluded as being responsible for transient bleaching under these conditions.

One possible scenario to explain these spectral changes would involve the photochemical dissociation not of the cysteinate anion, but instead a cysteine radical $CysS^\bullet$ via homolytic cleavage of a Fe–S bond, and the corresponding recombination of the intermediate species (eq 12). The modest decrease in k_2 with increasing $[Cys]_{tot}$ (Table S-6) may be due to the reversible adduct formation between $CysS^\bullet$ and $CysS^-$.[28]

Notably, the relaxation process seen for the flash photolysis studies in pH 10 solution appeared not to be fully reversible during the time frame of the experiment (Figures 11 and S-6). Furthermore, long-term repetitive photolysis with the pulsed

$$Fe(CysS)_2(NO)_2^- \xrightleftharpoons[k_2]{h\nu} Fe(CysS)(NO)_2^- + CysS^\bullet \quad (12)$$

laser (355 nm) led to net change observed as in the solution spectrum, most prominently decreased absorbance over the 340–500 nm range (SI Figure S-9), when the solution was photolyzed with magnetic stirring in a Schlenk photolysis cell.[20] Possible explanations for this irreversibility would be dimerization of the $CysS^\bullet$ radical to $(CysS)_2$ or trapping of this species by NO to form the S-nitrosothiol CysSNO. Surprisingly, when this solution was shaken manually, the spectrum of the photolyzed sample nearly returns to that seen before photolysis. We see no obvious explanation for this phenomenon other than the possibility that exposure of the solution to longer wavelength room light decomposed S-nitrosothiols to the RS· radical plus NO,[29,30] thereby providing a pathway for restoration of **Cys-DNIC**.

SUMMARY

Dinitrosyl iron complexes, especially those involving thiols, have been argued to be the most common form of nitric oxide equivalents in mammalian physiology.[10] DNICs are formed by the reaction of Fe^{2+} in the chelatable (labile) iron pool with NO and biological thiols, and these reactions are generally argued to be quite rapid.[7,12] While the majority of these are likely to be protein bound,[31] more mobile forms such as **Cys-DNIC** and its glutathione analog may play important roles in the transport of this functionality through the cell.[12] Various reactivities have been attributed to DNICs, including a role in the formation of another biological reservoir of NO, the S-nitrosothiols.[7,32] It is clear that there is a marked interplay between all these species in mammalian biology.

The investigations described here have used temporal changes in the optical spectra to outline the dynamics of DNIC formation from solutions of iron(II), the thiol cysteine, and nitric oxide in aqueous solutions of various pH values. As observed previously by Vanin and co-workers[9] the dinuclear Roussin's red ester **Cys-RSE** is formed at low pH, while the mononuclear complex **Cys-DNIC** is formed in alkaline media. The nature of the latter species was confirmed by EPR experiments. Notably all these reactions were carried out under deaerated conditions. At the near neutral pH 7.4, **Cys-RSE** is formed at relatively low total cysteine concentrations, but the transformation to **Cys-DNIC** occurs readily when additional CysSH is introduced. The kinetics of DNIC formation at 298 K are also strongly pH dependent and demonstrate a second-order dependence on the total cysteine concentration $[Cys]_{tot}$. The rapid biological formation of DNICs can thus be attributed to the high concentration of thiols in cells (especially glutathione at 0.5–10 mM).[33] Notably, the studies here were at 25 °C, so one might expect larger values of key rate constants such as the k_r for eq 5 (Scheme 1) at physiological temperatures.

Based on these data we have proposed a mechanism for DNIC formation from components that, regardless of the eventual product under these conditions, proceeds through pH-dependent formation of a common mononuclear intermediate $Fe^{II}(CysS)_2(NO)(H_2O)_x$. Spontaneous decomposition of this species, presumably accompanied by formation of the radical $CysS^\bullet$, would give the Fe(I) precursors of both **Cys-RSE** and **Cys-DNIC** (Scheme 2). That such precursors are quite labile is

dx.doi.org/10.1021/ja510393q | J. Am. Chem. Soc. 2015, 137, 328–336

illustrated by flash photolysis studies that demonstrated that reaction of the unsaturated dinuclear complex $Fe_2(\mu\text{-CysS})_2(NO)_3$ with NO (eq 10) proceeds with a second-order rate constant k_{NO} of 6.9×10^7 M^{-1} s^{-1}. Interestingly, flash photolysis of **Cys-DNIC** did not labilize NO but instead apparently leads to a reversible photoredox reaction.

Notably, in pH 7.4 solution, the dinuclear DNIC **Cys-RSE** undergoes a reaction first-order in added CysSH to form **Cys-DNIC**, further demonstrating the labilities of these systems. By such studies, we have begun the task of mapping the dynamics landscape defining the key transformations interlinking these labile and biologically relevant metal centers.

EXPERIMENTAL SECTION

Materials. L-Cysteine (≥98.0%) and iron(II) sulfate heptahydrate (>99.0%) were purchased from Sigma. Nitric oxide gas (99.5%) from the tank (PraxAir) was purified to remove NO_2 and N_2O_3 by passing through a stainless steel column containing Ascarite II (Sigma).[34]

Solutions at pH 5.0 and 5.6 were prepared in citrate buffer (citrate tribasic dehydrate, ≥99.0%), those at pH 6.8 and 7.4 were prepared in HEPES (≥99.5%) buffer, and those at pH 9.0 and 10.0 are prepared in borate buffer (sodium borate decahydrate, ≥99.0%). Schlenk quartz cuvettes[20] were used to prepare anaerobic solutions for recording the absorption spectra of **Cys-RSE** and **Cys-DNIC** and for the kinetics studies on microsecond time scale using laser photolysis. The initial buffered solutions (5 mL) in the cuvette contained the desired concentrations of cysteine and of iron(II) sulfate. These were deoxygenated by the use of the freeze−pump−thaw (3×) method. Measured amounts of NO gas were then added to the cell (either by using a vacuum line and a monometer or using a gastight syringe depending on the experiment) to give the desired NO concentrations calculated according to the partition coefficient between the liquid and gas phases.[21]

Computations. The structures of iron cysteine nitrosyl complexes were optimized using unrestricted approach with B3LYP functional and the full-electron, DFT-optimized, double ζ + valence polarization basis set equivalent to the DZVP basis set used in DGauss software (DGDZVP), inside the Gaussian 09 package. All calculations were performed without symmetry constraints. The starting geometries around iron were either pseudotetrahedral or pseudo-octahedral in which all coordination sites were occupied by NO, cysteinate ion, and the remainder by water molecules. The lowest energy spin states were determined in vacuum, and then these molecules were optimized again using the polarized continuum model (PCM, solvent = water) also at UB3LYP/DGDZVP theory level.

Instrumental Methods. Optical absorbance measurements were recorded using a Shimadzu dual beam UV-2401 PC spectrophotometer in 1.00 cm path-length quartz cells. Stopped-flow kinetics studies for reactions completed on the time frame of ms to s were measured using an Applied Photophysics model SX-18 MV spectrophotometer. Oxygen was removed from the stopped-flow mechanism by vacuum pumping for 1 h. Deaerated solutions were prepared in an inert atmosphere box or by vacuum line Schlenck techniques and transferred to the stopped-flow system using gastight Hamilton syringes with Luer locks. The temperature of the reaction system was controlled with a thermostated, circulating water bath. The results of the stopped-flow kinetics data were evaluated using the SX-18 software.

The laser flash photolysis apparatus and technique have previously been described in detail.[35] Briefly, solution samples in Schlenck quartz cells were photolyzed using the third harmonic (excitation wavelength λ_{ex} 355 nm) output of a Spectra-Physics INDI-HG Nd:YAG pulse laser. The laser excitation energy was ∼10 mJ/pulse with a pulse duration of ∼10 ns. The probe beam, perpendicular to the excitation beam, was the output of a 300 W xenon lamp, passed through an IR filter and a SPEX (1681 Spectrometer) monochromator (to select the probe wavelength) prior to the sample combined with a second SPEX (1681 Spectrometer) monochromator (to filter scattered laser pulse light) prior to a 1P28 photomultiplier tube (PMT). Signals from the PMT were recorded on a LeCroy digital oscilloscope (LT342), and each kinetic trace was an average of 50 traces. The kinetics was analyzed using Matlab and Origin software.

The EPR spectra were recorded using a Bruker EMX Plus EPR spectrometer, operating in the X-band frequencies, with a field modulation of 100 kHz at room temperature. The microwave power and the amplitude modulation were kept at 20 mW and 0.05 or 0.2 mT. During the spectrum recording, sweep time and time constant were 15.36 s and 5.12 ms, respectively. The samples were measured in a 1 mm capillary tube in the absence of oxygen.

ASSOCIATED CONTENT

Supporting Information

One scheme, six tables, and nine figures provide additional documentation of the studies described in this manuscript. This material is available free of charge via the Internet at http://pubs.acs.org/.

AUTHOR INFORMATION

Corresponding Authors

rmhan@chem.ruc.edu.cn

ford@chem.ucsb.edu

Notes

The authors declare no competing financial interest.

ACKNOWLEDGMENTS

J.C.M.P. acknowledges the fellowship support from Conselho Nacional de Desenvolvimento Científico e Tecnológico - National Counsel of Technological and Scientific Development. R.-M.H. acknowledges the financial support from China Scholarship Council. This work was supported by grants to PCF from US National Science Foundation (CHE-1058794 and CHE-1405062). We acknowledge support from the Center for Scientific Computing from the CNSI, MRL: an NSF MRSEC (DMR-1121053) and NSF CNS-0960316. We thank Prof. D. W. Franco for EPR measurements.

REFERENCES

(1) Ignarro, L. J. *Nitric Oxide: Biology and Pathobiology*, 2nd ed.; Elsevier Inc.: Burlington, MA, 2010.

(2) Toledo, J.; Bosworth, C. A.; Hennon, S. W.; Mahtani, H. A.; Bergonia, H. A.; Lancaster, J. R. *J. Biol. Chem.* **2008**, *283*, 28926−28933.

(3) Lancaster, J. R., Jr.; Hibbs, J. B. *Proc. Nat. Acad. Sci. U.S.A.* **1990**, *87*, 1223−1227.

(4) Vedernikov, Y. P.; Mordvintcev, P. I.; Malenkova, I. V.; Vanin, A. F. *Eur. J. Pharmacol.* **1992**, *211*, 313−317.

(5) Kim, Y. M.; Chung, H. T.; Simmons, R. L.; Billiar, T. R. *J. Biol. Chem.* **2000**, *275*, 10954−10961.

(6) (a) Butler, A. R.; Megson, I. L. *Chem. Rev.* **2002**, *102*, 1155−1165. (b) Much earlier studies of dinitrosyl studies are summarized in this important review.

(7) (a) Bosworth, C. A.; Toledo, J. C., Jr.; Zmijewski, J. W.; Li, Q.; Lancaster, J. R., Jr. *Proc. Natl. Acad. Sci. U.S.A.* **2009**, *106*, 54671−4676. (b) Li, Q.; Li, C.; Mahtani, H. K.; Du, J.; Patel, A. R.; Lancaster, J. R. *J. Biol. Chem.* **2014**, *289*, 19917−19927.

(8) (a) Harrop, T. C.; Song, D.; Lippard, S. J. *J. Am. Chem. Soc.* **2006**, *128*, 3528−3529. (b) Tonzetich, Z. J.; McQuade, L. E.; Lippard, S. J. *Inorg. Chem.* **2010**, *49*, 6338−6348.

(9) (a) Vanin, A. F.; Poltorakov, A. P.; Mikoyan, V. D.; Kubrina, L. N.; Burbaev, D. S. *Nitric Oxide* **2010**, *23*, 136−149. (b) Borodulin, R. R.; Kubrina, L. N.; Serezhenkov, V. A.; Burbaev, D. S.; Mikoyan, V. D.; Vanin, A. F. *Nitric Oxide* **2013**, *35*, 35−41. (c) Vanin, A. F.; Papina, A. A.; Serezhenkov, V. A.; Koppenol, W. H. *Nitric Oxide* **2004**, *10*, 60−73.

(10) Hickok, J. R.; Sahni, S.; Shen, H.; Arvind, A.; Antoniou, C.; Fung, L. W. M.; Thomas, D. D. *Free Radical Biol. Med.* **2011**, *51*, 1558−1566.
(11) (a) Lu, T.-T.; Tsou, C.-C.; Huang, H.-W.; Hsu, I.-J.; Chen, J.-M.; Kuo, T.-S.; Wang, Y.; Liaw, W.-F. *Inorg. Chem.* **2008**, *47*, 6040−6050. (b) Chen, Y.-J.; Ku, W.-C.; Feng, L.-T.; Tsai, M.-L.; Hsieh, C.-H.; Hsu, W.-H.; Liaw, W.-F.; Hung, C.-H.; Chen, Y.-J. *J. Am. Chem. Soc.* **2008**, *130*, 10929−10938. (c) Lin, Z.-S.; Lo, F.-C.; Li, C.-H.; Chen, C.-H.; Huang, W.-N.; Hsu, I.-J.; Lee, J.-F.; Horng, J.-C.; Liaw, W.-F. *Inorg. Chem.* **2011**, *50*, 10417−10431. (d) Lu, C.-Y.; Liaw, W.-F. *Inorg. Chem.* **2013**, *52*, 13918−13926. (e) Tsou, C.-C.; Chiu, W.-C.; Ke, C.-H.; Tsai, J.-C.; Wang, Y.-M.; Chiang, M.-H.; Liaw, W.-F. *J. Am. Chem. Soc.* **2014**, *136*, 9424−9433.
(12) Lok, H. C.; Rahmanto, Y. S.; Hawkins, C. L.; Kalinowski, D. S.; Morrow, C. S.; Townsend, A. J.; Ponka, P.; Richardson, D. R. *J. Biol. Chem.* **2012**, *287*, 607−618.
(13) (a) Pulukkody, R.; Kyran, S. J.; Bethel, R. D.; Hsieh, C.-H.; Hall, M. B.; Darensbourg, D. J.; Darensbourg, M. Y. *J. Am. Chem. Soc.* **2013**, *135*, 8423−8430. (b) Hsieh, C.-H.; Brothers, S. M.; Reibenspies, J. H.; Hall, M. B.; Popescu, C. V.; Darensbourg, M. Y. *Inorg. Chem.* **2013**, *52*, 2119−2124. (c) Pinder, T. A.; Montalvo, S. K.; Hsieh, C.-H.; Lunsford, A. M.; Bethel, R. D.; Pierce, B. S.; Darensbourg, M. Y. *Inorg. Chem.* **2014**, *53*, 9095−9105.
(14) (a) Nhut, G. T.; Kalyvas, H.; Skodje, K. M.; Hayashi, T.; Moenne-Loccoz, P.; Callan, P. E.; Shearer, J.; Kirschenbaum, L. J.; Kim, E. *J. Am. Chem. Soc.* **2011**, *133* (5), 1184−1187. (b) Tran, C. T.; Kim, E. *Inorg. Chem.* **2012**, *51*, 10086−10088. (c) Skodje, K. M.; Kwon, M.-Y.; Chung, S. W.; Kim, E. *Chem. Sci.* **2014**, *5*, 2374−2378. (d) Fitzpatrick, J.; Kalyvas, H.; Filipovic, M. R.; Ivanovic-Burmazovic, I.; MacDonald, J. C.; Shearer, J.; Kim, E. *J. Am. Chem. Soc.* **2014**, *136*, 7229−7232.
(15) Ford, P. C.; Pereira, J. C. M.; Miranda, K. M. *Struct. Bonding (Berlin)* **2014**, *154*, 99−135.
(16) Conrado, C. L.; Bourassa, J. L.; Egler, C.; Wecksler, S.; Ford, P. C. *Inorg. Chem.* **2003**, *42*, 2288−2293.
(17) Costanzo, S.; Ménage, S.; Purrello, R.; Bonomo, R. P.; Fontecave, M. *Inorg. Chim. Acta* **2001**, *318*, 1−7.
(18) (a) Vanin and coworkers have assigned the DNIC displaying the EPR g_{ave} = 2.03 signature as being $[Fe^{I}(NO^{+})_2L_2]^{n+}$ (or formally $[Fe^{III}(NO)_2L_2]^{n+}$) in character ($\{Fe(NO)_2\}^7$ in Enemark/Feltham notation, ref 18b). However, others have demonstrated with crystallographically characterized complexes (refs 13b and 18c) that this g_{ave} = 2.03 signature defines a $\{Fe(NO)_2\}^9$ species, such as the $[Fe^{I}(NO)_2(CysS)_2]^{-}$ anion that we have assigned as the mononuclear DNIC in this case. Notably, the Roussin's red salt esters are also clearly $Fe^{I}(NO)_2$ in character, although they are diamagnetic owing to coupling between the two iron centers. (b) Enemark, J. H.; Feltham, R. D. *Coord. Chem. Rev.* **1974**, *13*, 339−406. (c) Tsou, C.-C.; Tsai, F. T.; Chen, H.-Y.; Hsu, I.-J.; Liaw, W. F. *Inorg. Chem.* **2013**, *52*, 1631−1639.
(19) Following the comments in ref 18a, the aqueous anionic mononitrosyl iron complex $[Fe^{I}(NO)(CysS)_2]^{-}$ would be a $\{Fe(NO)\}^8$ species (ref 18b).
(20) (a) A Schlenck cuvette has the optical cell fused to a small all-glass apparatus designed for attaching to vacuum lines for preparing deaerated solutions of reactive gases in equilibrium with a gas phase volume of ∼20 mL. A diagram of this apparatus is shown in the Supporting Information of ref 17b. (b) Rimmer, R. D.; Richter, H.; Ford, P. C. *Inorg. Chem.* **2010**, *49*, 1180−1185.
(21) Battino, R. *IUPAC: Solubility Data Series*; Pergamon Press: New York, 1981; Vol. 7, p 452.
(22) (a) Wanat, A.; Schneppensieper, T.; Stochel, G.; van Eldik, R.; Bill, E.; Wieghardt, K. *Inorg. Chem.* **2002**, *41*, 4−10. (b) The K_{NO} value of 1.15 × 10^3 M^{-1} reported by ref 22a was measured using an NO-sensitive electrode. Values determined by van Eldik et al. using a flash photolysis kinetics technique (22a,c) fell in the range 440−500 M^{-1} that were very close to the K_{NO} values reported by temperature jump kinetics method (22d,e). (c) Schneppensieper, T.; Wanat, A.; Czap, A.; Stochel, G.; Goldstain, S.; Meyerstein, D.; van Eldik, R. *Eur. J. Inorg. Chem.* **2001**, 2317. (d) Littlejohn, D.; Chang, S. G. *J. Phys. Chem.* **1982**, *86*, 537. (e) Kustin, K.; Taub, I. A.; Weinstock, E. *Inorg. Chem.* **1966**, *5*, 1079.
(23) (a) Kudrik, E. V.; van Eldik, R.; Makarov, S. V. *Dalton Trans.* **2004**, 429−435. (b) Schneppensieper, T.; Wanat, A.; Stochel, G.; van Eldik, R. *Inorg. Chem.* **2002**, *41*, 2565−2573.
(24) (a) Ford, P. C.; Fernandez, B. O.; Lim, M. D. *Chem. Rev.* **2005**, *105*, 2439−2455. (b) Fernandez, B. O.; Lorkovic, I. M.; Ford, P. C. *Inorg. Chem.* **2004**, *43*, 5393−5402.
(25) Dawson, R. M. C. *Data for Biochemical Research*, 3rd ed.; Clarendon Press: Oxford, 1986.
(26) Tinberg, C. E.; Tonzetich, Z. J.; Wang, H.; Do, L. H.; Yoda, Y.; Cramer, S. P.; Lippard, S. J. *J. Am. Chem. Soc.* **2010**, *132*, 18168−1817.
(27) Bourassa, J.; Ford, P. C. *Coord. Chem. Rev.* **2000**, *200*, 887−900.
(28) Wardman, P.; Von Sonntag, C. *Methods Enzymol.* **1995**, *251*, 31−55.
(29) Andreasen, L. V.; Lorkovic, I. M.; Richter-Addo, G. B.; Ford, P. C. *Nitric Oxide* **2002**, *6*, 228−235.
(30) Shishido, S. M.; Seabra, A. B.; Loh, W.; de Oliveira, M.G. *Biomaterials* **2003**, *24*, 3543−3553.
(31) De Maria, F.; Pedersen, J. Z.; Caccuri, A. M.; Antonini, G.; Turella, P.; Stella, L.; Lo Bello, M.; Federici, G.; Ricci, G. *J. Biol. Chem.* **2003**, *278*, 42283−42293.
(32) Cesareo, E.; Parker, L. J.; Pedersen, J. Z.; Nuccetelli, M.; Mazzetti, A. P.; Pastore, A.; Federici, G.; Caccuri, A. M.; Ricci, G.; Adams, J. J.; Parker, M. W.; Lo, B. *J. Biol. Chem.* **2005**, *280*, 42172−42180.
(33) Maher, P. *Ageing Res. Rev.* **2005**, *4*, 288−314.
(34) Lim, M. D.; Lorkovic, I. M.; Ford, P. C. *Methods Enzymol.* **2005**, *396* (Part E), 3−17.
(35) Dethlefsen, J. W.; Hedegard, E. D.; Rimmer, R. D.; Ford, P. C.; Doessing, A. *Inorg. Chem.* **2009**, *48*, 231−238.